Journal of Zhejiang University-SCIENCE A (Applied Physics & Engineering)
ISSN 1673-565X (Print); ISSN 1862-1775 (Online)
www.zju.edu.cn/jzus; www.springerlink.com
E-mail: jzus@zju.edu.cn

Stress intensity factors under combined bending and torsion moments

Al Emran ISMAIL[†1,2], Ahmad Kamal ARIFFIN[2], Shahrum ABDULLAH[2], Mariyam Jameelah GHAZALI[2], Mohammed ABDULRAZZAQ[2], Ruslizam DAUD[3]

([1]*Faculty of Mechanical & Manufacturing Engineering, Universiti Tun Hussein Onn Malaysia, Batu Pahat 86400, Johor, Malaysia*)

([2]*Faculty of Engineering & Built Environment, Universiti Kebangsaan Malaysia, Bangi 43600, Selangor, Malaysia*)

([3]*School of Mechatronic Engineering, Universiti Malaysia Perlis, Arau 02600, Perlis, Malaysia*)

[†]E-mail: emran@uthm.edu.my

Received Feb. 20, 2011; Revision accepted May 19, 2011; Crosschecked Dec. 6, 2011

Abstract: This paper discusses stress intensity factor (SIF) calculations for surface cracks in round bars subjected to combined torsion and bending loadings. Different crack aspect ratios, a/b, ranging from 0.0 to 1.2 and relative crack depths, a/D, ranging from 0.1 to 0.6 were considered. Since the loading was non-symmetrical for torsion loadings, a whole finite element model was constructed. Then, the individual and combined bending and torsion loadings were remotely applied to the model. The equivalent SIF method, F^*_{EQ}, was then used explicitly to combine the individual SIFs from the bending and torsion loadings. A comparison was then carried out with the combined SIF, F^*_{FE}, obtained using the finite element analysis (FEA) under similar loadings. It was found that the equivalent SIF method successfully predicted the combined SIF for Mode I. However, discrepancies between the results determined from the different approaches occurred when F_{III} was involved. It was also noted that the predicted F^*_{FE} using FEA was higher than the F^*_{EQ} predicted through the equivalent SIF method due to the difference in crack face interactions.

Key words: Stress intensity factor (SIF), Combined loadings, Finite element analysis (FEA), Surface cracks, Round solid bars
doi:10.1631/jzus.A1100040 **Document code:** A **CLC number:** O39

1 Introduction

Round bars are generally used to transmit power from one component to another (Carpinteri, 1992; 1993). These components are subjected to fatigue stresses which can cause mechanical damage and premature failure. The initiation of fatigue cracks on the surface is usually due to mechanical defects, such as notches (Alshoaibi and Ariffin, 2006; Alshoaibi *et al.*, 2007; Ismail *et al.*, 2011) and metallurgical defects (Gray *et al.*, 1985). In service, a rotating shaft is generally subjected to a combined loading due to its self-weight, which induces a bending moment, and torsion loadings. In fact, any arbitrary shapes of crack initiation may grow and take a semi-elliptical shape (Lin and Smith, 1997). Then, linear elastic fracture mechanics (LEFM) has been used to analyze stress intensity factors (SIFs) along the crack front. The solution of SIFs for a wide range of geometries under Mode I loadings has been reported (Raju and Newman, 1986; Carpinteri, 1992; Fonte and Freitas, 1999; Carpinteri *et al.*, 2006; Mahmoud, 2007). However, the calculation of SIFs for bars subjected to Mode III loadings and that of SIFs under combined loadings, such as bending and torsion, have rarely been studied (Fonte and Freitas, 1999; Shahani and Habibi, 2007).

Therefore, the aim of this study was to obtain the SIFs for semi-elliptical surface cracks subjected to a bending moment, a torsion moment and the combination of bending and torsion loadings. This work was also carried out to investigate whether the SIFs from different modes could be explicitly combined using the superposition or equivalent SIF methods. The results from these methods were compared with the SIF

obtained using finite element analysis (FEA) under combined bending and torsion loadings. Finally, the discrepancies between the two methods are discussed in terms of mesh deformation, focusing mainly on crack face interactions.

2 Evaluation of stress intensity factors

The finite element method (FEM) is an appropriate method to calculate the SIF for linear elastic fracture mechanics problems. To determine the SIFs, a displacement extrapolation method (ANSYS, 2007) was used in this study. Several other published methods were also available (Aslantas, 2003; Agrawal and Karlsson, 2006; Aslantas *et al.*, 2006). Fig. 1 shows the arbitrary crack shape where the crack face is parallel to the *x*- and *z*-axis is normal to the *x*-*y* plane. The displacement components in *x*-, *y*- and *z*-axis are represented by *u*, *v* and *w*, respectively. Local polar coordinates (r,θ) originated at the crack tip are used to predict the stress distributions around the crack front.

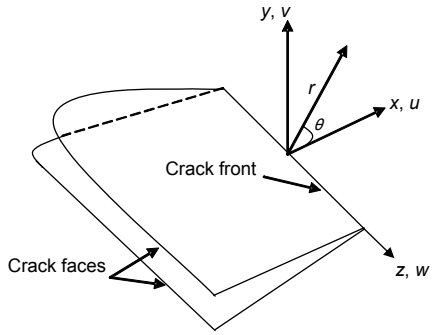

Fig. 1 Arbitrary crack shape

Fig. 2 shows the arrangement of singular finite elements around the crack tip used in this work where points *c* and *d* are the quarter distance from point *e* (crack tip) and *L* is the length of element. After obtaining the elastic finite element solution of the particular problem, nodal displacements between two crack faces were determined and used to compute the SIFs as follows:

$$K_{\mathrm{I}}=\frac{2G\sqrt{2\pi}}{1+\kappa}\frac{|v_c-v_d|}{\sqrt{r}}=\frac{2G\sqrt{2\pi}}{1+\kappa}\frac{|\Delta v|}{\sqrt{r}}, \quad (1)$$

$$K_{\mathrm{II}}=\frac{2G\sqrt{2\pi}}{1+\kappa}\frac{|u_c-u_d|}{\sqrt{r}}=\frac{2G\sqrt{2\pi}}{1+\kappa}\frac{|\Delta u|}{\sqrt{r}}, \quad (2)$$

$$K_{\mathrm{III}}=2G\sqrt{2\pi}\frac{|w_c-w_d|}{\sqrt{r}}=2G\sqrt{2\pi}\frac{|\Delta w|}{\sqrt{r}}, \quad (3)$$

where K_{I}, K_{II} and K_{III} are the Mode I, II and III SIFs, respectively, Δv, Δu and Δw are the relative nodal displacements between two crack faces in the direction of *y*-, *x*- and *z*-axis, respectively, and *G* is the modulus of rigidity. For plain strain condition, $\kappa=3-4\nu$, where ν is Poisson's ratio.

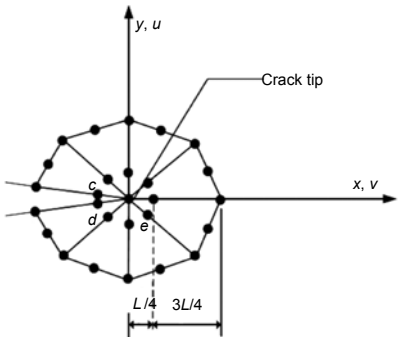

Fig. 2 Singular elements around the crack tip

3 Finite element modeling

A circular cross-section of a component with a surface crack is shown in Fig. 3 (Toribio *et al.*, 2008). The geometry of the crack can be described by the dimensionless *a*/*D* and *a*/*b*, the so-called relative crack depth and crack aspect ratios, where *D*, *a* and *b* are the diameter of the bar, the crack depth and the major diameter of the ellipse, respectively. Any arbitrary points on the crack front can also be normalized as *x*/*h*, where *h* is the crack width, and *x* is the arbitrary distance of point *P* from the symmetry axis. The outer diameter of the cylinder was 50 mm and the total length was 200 mm. Due to the non-symmetrical analysis involved, a full finite element model was constructed, in which the surface crack was situated at the centre of the cylinder.

In addition, a finite element model was developed using the ANSYS software with special attention given to the crack tip by employing 20-node iso-parametric quadratic brick elements. The square-root singularities of stresses and strains were modeled by shifting the mid-point nodes to the quarter-point locations around the crack-tip region. The detail of the finite element model is shown in Fig. 4 with the associated singular finite elements around the crack tip.

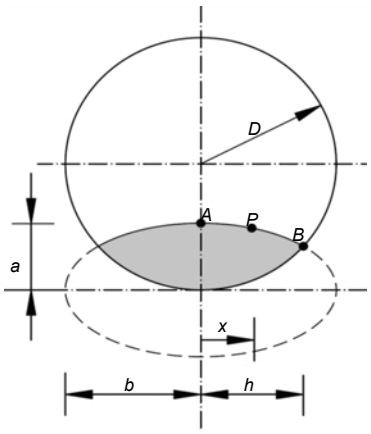

Fig. 3 Nomenclature of a semi-elliptical surface crack

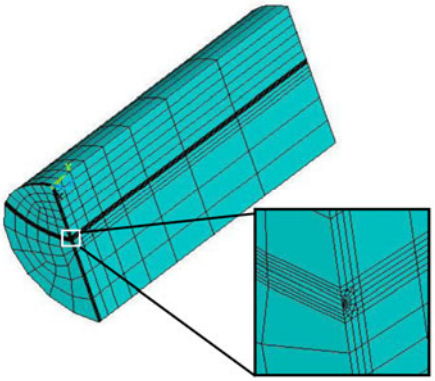

Fig. 4 Symmetrical finite element model

To remotely apply loadings to the structural component, a rigid element or multi-point constraint (MPC) elements were used to connect the nodes at a circumferential line at the end of the component, to an independent node. Fig. 5 shows a technique for constructing the independent node connected to the model using rigid beam elements. The bending moment, M_y, and the torsion moment, T_x, were directly applied to this node, whereas the axial force was directly applied in the x-direction on the cross-sectional area of the bar.

At the other end, the component was fully constrained in all degrees of freedom. All the SIFs obtained from the analysis were converted into normalized values to ensure the generality of the results. A normalized SIF, F, can be defined as follows (Fonte and Freitas, 1999):

$$F_{\mathrm{I}}=\frac{K_{\mathrm{I}}}{\sigma_x\sqrt{\pi a}}, \tag{4}$$

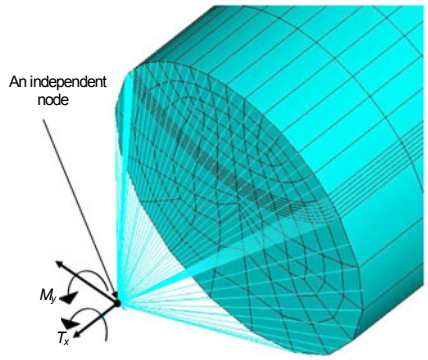

Fig. 5 Remotely applied moments using an MPC184 element

$$F_{\mathrm{II}}=\frac{K_{\mathrm{II}}}{\tau_{xy}\sqrt{\pi a}}, \tag{5}$$

$$F_{\mathrm{III}}=\frac{K_{\mathrm{III}}}{\tau_{xy}\sqrt{\pi a}}, \tag{6}$$

where K_{I} are the SIFs under bending or the axial stress, σ_x, and K_{II} or K_{III} are the SIFs under shear stress, τ_{xy}. Two loading ratios can be written as

$$\vartheta=\frac{\sigma_{\mathrm{b}}}{\sigma_{\mathrm{a}}}, \tag{7}$$

$$\gamma=\frac{\tau_{xy}}{\sigma_{\mathrm{b}}}, \tag{8}$$

where ϑ is the loading ratio between the bending stress, σ_{b}, and the axial stress, σ_{a}, whereas γ is the ratio between the shear stress, τ_{xy}, and the bending stress, σ_{b}. The three values of both ratios were 0.5, 1.0 and 2.0.

To obtain a suitable finite element model, it was necessary to compare the proposed model with other published models (Carpinteri *et al.*, 2006; Toribio *et al.*, 2008; Carpinteri and Vantadori, 2009). Fig. 6

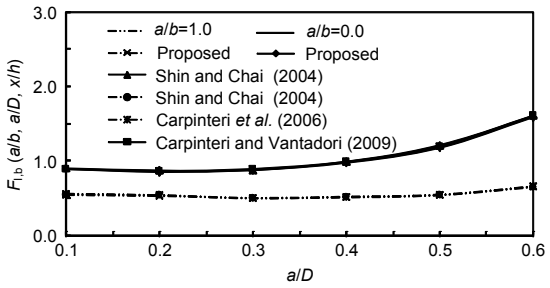

Fig. 6 Comparison and validation of the proposed finite element model with the previous results

shows a comparison of the dimensionless SIFs under bending moment, $F_{I,b}$. The findings of this study are in good agreement with those of previous models. Until now, the solution of Mode III SIFs has been difficult to obtain (Fonte and Freitas, 1999; Shahani and Habibi, 2007). We concluded that the model developed in this study was capable of analyzing Mode III condition.

4 Stress intensity factors under different loadings

Figs. 7 to 9 show the dimensionless SIFs, $F_{I,b}$, F_{II} and F_{III} respectively, along the crack front under pure bending and torsion moments for the selected crack conditions. The SIFs were calculated at every point along the crack front. However, the SIF at the intersection between the crack and the surface was not determined due to the square-root singularity problem. Also, the use of a quarter point finite element did not generally produce reliable results for the outer intersection surface. The nearest point was approximately 83% from where x/h=0.0 or the deepest point. When the x/h point approached the outer surface of the bar, $F_{I,b}$ was found to be slightly higher than other values. It was clearly shown that the maximum $F_{I,b}$ always occurred at the intersection point area.

Under bending moment, the crack growth started at the intersection point and the semi-elliptical crack front sometimes flattened as the cracks grew (Lin and Smith, 1997). For the case of a/b=1.2, $F_{I,b}$ was not strongly affected by a/D, whereas $F_{I,b}$ seemed to converge at a certain value, particularly when $a/D\leq$ 0.5. When $F_{I,b}$ reached $x/h\geq$0.6, $F_{I,b}$ diverged to its individual maximum value but the maximum value still occurred at the outer surface of the bar.

At x/h=0.0, F_{II}=0 (Fig. 8) and it increased steeply to the intersection point. Fig. 9 shows F_{III} along the crack front subjected to torsion loading. The effect on F_{III} was strongly related to the relative crack depth, a/D. For a/D<0.3, the maximum F_{III} occurred at the deepest point in the crack, and when a/D>0.3, the maximum F_{III} was shifted to the intersection surface area. The transition x/h was observed when a/b increased to the outer edge of the bar, implying different crack evolutions could be obtained during crack growth.

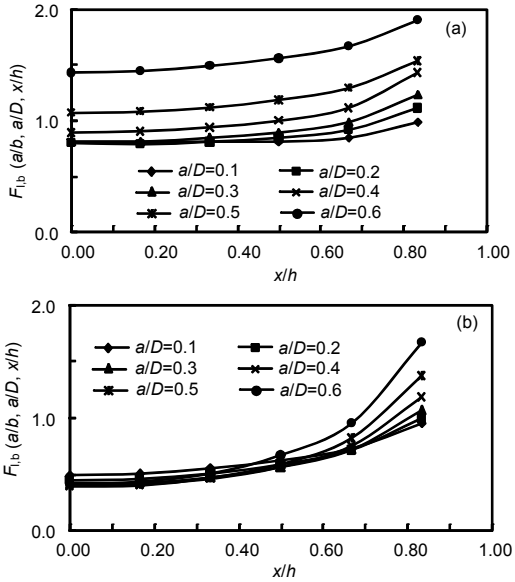

Fig. 7 Behavior of normalized stress intensity factors under bending moment, $F_{I,b}$ against normalized coordinates, x/h for two crack aspect ratios (a) a/b=0.4 and (b) a/b=1.2

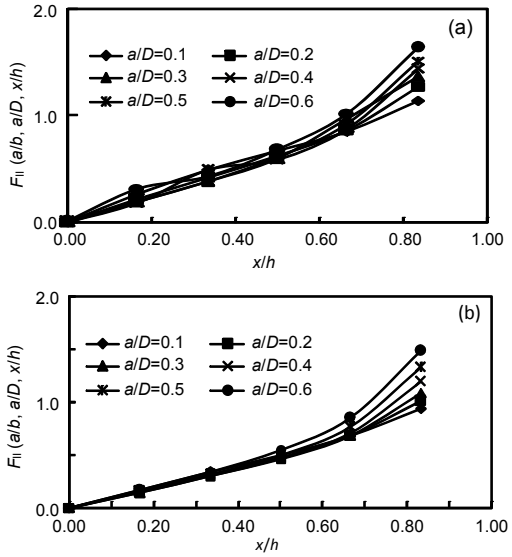

Fig. 8 Behavior of normalized stress intensity factors under torsion moment, F_{II} against normalized coordinates, x/h for two crack aspect ratios (a) a/b=0.4 and (b) a/b=1.0

5 Stress intensity factors under combined loadings

In previous studies (Fonte and Freitas, 1999; Shahani and Habibi, 2007), it is hard to find the SIFs under combined loadings. This is because it was assumed that all normalized SIFs could be obtained

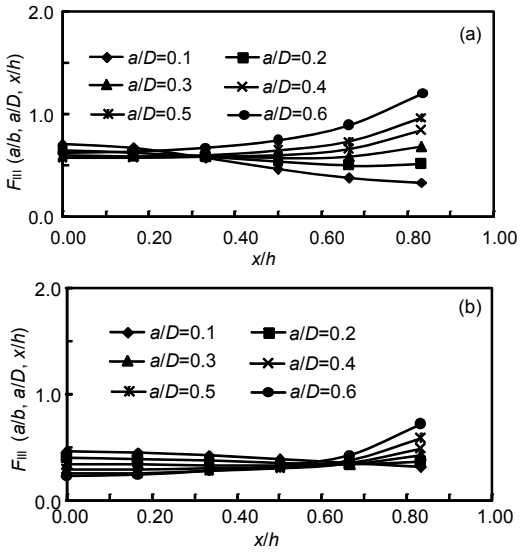

Fig. 9 Behavior of normalized stress intensity factors under torsion moment, F_{III} against normalized coordinates, x/h for two crack aspect ratios (a) a/b=0.4 and (b) a/b=1.0

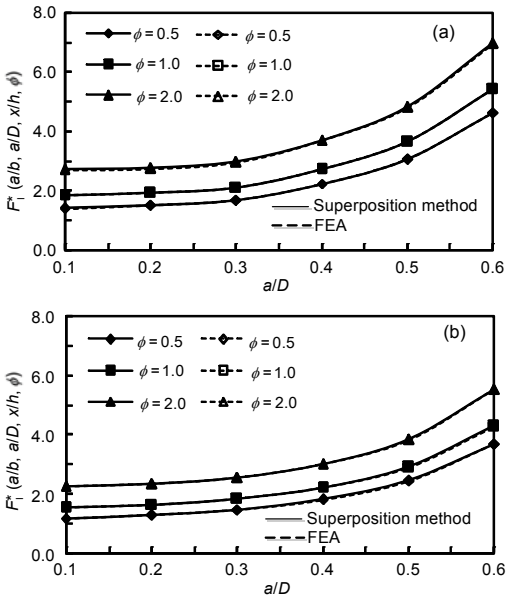

Fig. 10 Comparisons of normalized stress intensity factors under combined loadings, F^* plotted against relative crack depths, a/D for two crack aspect ratios, (a) a/b=0.2 and (b) a/b=0.6 obtained at x/h=0.0

using the superposition technique. This assumption was established for a similar type of loading mode, for example Mode I (Raju and Newman, 1986). The combined SIF, F^*_{EQ}, under Mode I loadings are here obtained by the superposition method through Eq. (9) defined as

$$F^*_{EQ} = F_{I,a} + \vartheta F_{I,b}. \tag{9}$$

Then, these combined SIFs are compared with the combined SIFs, F^*_{FEA}, obtained using FEA, with excellent agreement (Fig. 10).

Further modification of the superposition technique was required to include F_{II} and F_{III}. Therefore, the equivalent SIF method is used instead of a superposition method. The equivalent SIF is defined as (Qian and Fatemi, 1996)

$$K_{eqv} = \sqrt{K_I^2 + K_{II}^2 + \frac{K_{III}^2}{1-\nu}}, \tag{10}$$

where K_{eqv} is the equivalent SIF. It is assumed that $K_{eqv}=K^*_{EQ}$. Substituting Eqs. (4)–(6) into Eq. (10) yields

$$K^* = \sqrt{\left(F_{I,b}\sigma_x\sqrt{\pi a}\right)^2 + \left(F_{II}\tau_{xy}\sqrt{\pi a}\right)^2 + \left(\frac{F_{III}\tau_{xy}\sqrt{\pi a}}{1-\nu}\right)^2}. \tag{11}$$

Substituting Eq. (8) into Eq. (11), we can obtain

$$K^* = \sqrt{\left(\sigma_b\sqrt{\pi a}\right)^2\left[\left(F_{I,b}\right)^2 + \left(\gamma F_{II}\right)^2 + \left(\frac{\gamma F_{III}}{1-\nu}\right)^2\right]}. \tag{12}$$

Rearranging Eq. (12) in terms of combined dimensionless SIF, F^* is given by

$$F^* = \frac{K^*}{\sigma_b\sqrt{\pi a}} = \sqrt{\left(F_{I,b}\right)^2 + \left(\gamma F_{II}\right)^2 + \left(\frac{\gamma F_{III}}{1-\nu}\right)^2}. \tag{13}$$

Eq. (13) can be divided into two separate equations given as

$$F^*_{I,b-III,FE} = \frac{K^*_{FE}}{\sigma_b\sqrt{\pi a}}, \tag{14}$$

$$F^*_{I,b-III,EQ} = \sqrt{\left(F_{I,b}\right)^2 + \left(\gamma F_{II}\right)^2 + \left(\frac{\gamma F_{III}}{1-\nu}\right)^2}, \tag{15}$$

where $F^*_{I,b\text{-}III,FE}$ is the normalised SIF obtained directly from FEA, and $F^*_{I,b\text{-}III,EQ}$ is the normalised SIF obtained explicitly by combining the individual SIFs $F_{I,b}$, F_{II} and F_{III}. At x/h=0.0, F_{II}=0.0 (Fig. 8). To

simplify the problem in this study, our analysis focused only on this location. Therefore, Eq. (15) can be then reduced to the following expression:

$$F^*_{\mathrm{I,b-III,EQ}}=\sqrt{(F_{\mathrm{I}})^2+\left(\frac{\gamma F_{\mathrm{III}}}{1-\nu}\right)^2}. \tag{16}$$

Figs. 11a and 11b show $F_{\mathrm{I,b}}$ and F_{III}, respectively obtained at x/h=0.0 under bending and torsion moments. Then, $F_{\mathrm{I,b}}$ and F_{III} are combined explicitly through Eq. (16) using different stress ratio values, γ. It was hard to obtain a single value of SIF directly from ANSYS. Therefore, an elastic J-integral was used by assuming that a single value of J-integral under the combined loading represented the unified SIFs consisting of K_{I}, K_{II} and K_{III}. This is because in ANSYS, if J-integral is used in the elastic or plastic regions, it calculates only a single value of J-integral even under combined loadings. The elastic J-integral, J_{e}, can therefore be represented, as follows (Lei, 2004):

$$J_{\mathrm{e}}=\frac{K^2}{E}(1-\nu^2), \tag{17}$$

where E is the modulus of elasticity. Rearranging Eq. (17) in terms of SIF, K, yields

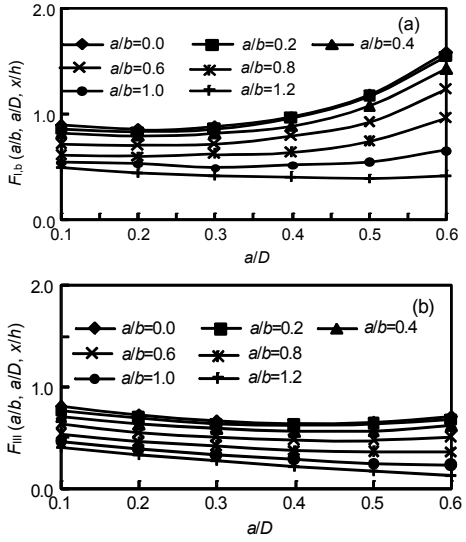

Fig. 11 Behavior of normalized stress intensity factors under (a) bending moment, $F_{\mathrm{I,b}}$ and (b) torsion moment, F_{III} obtained at x/h=0.0 plotted against relative crack depths, a/D

$$K^*_{\mathrm{FE}}=\sqrt{J_{\mathrm{e}}\left(\frac{E}{1-\nu^2}\right)}. \tag{18}$$

Eq. (18) was used to convert the J-integral into the combined SIF, K^*_{FE}, under combined loadings using FEA, and it was then substituted into Eq. (14).

$F^*_{\mathrm{I,b\text{-}III,EQ}}$ in Eq. (16) and $F^*_{\mathrm{I,b\text{-}III,FE}}$ from FEA in Eq. (14) were compared (Fig. 12). The discrepancies in $F^*_{\mathrm{I,b\text{-}III}}$ between the two approaches were determined largely by different values of a/b, a/D and x/h. In the case of a/b=0.2 (Fig. 12a), the combined SIF, $F^*_{\mathrm{I,b\text{-}III}}$ was successfully predicted and was in agreement with all values of loading ratios except for

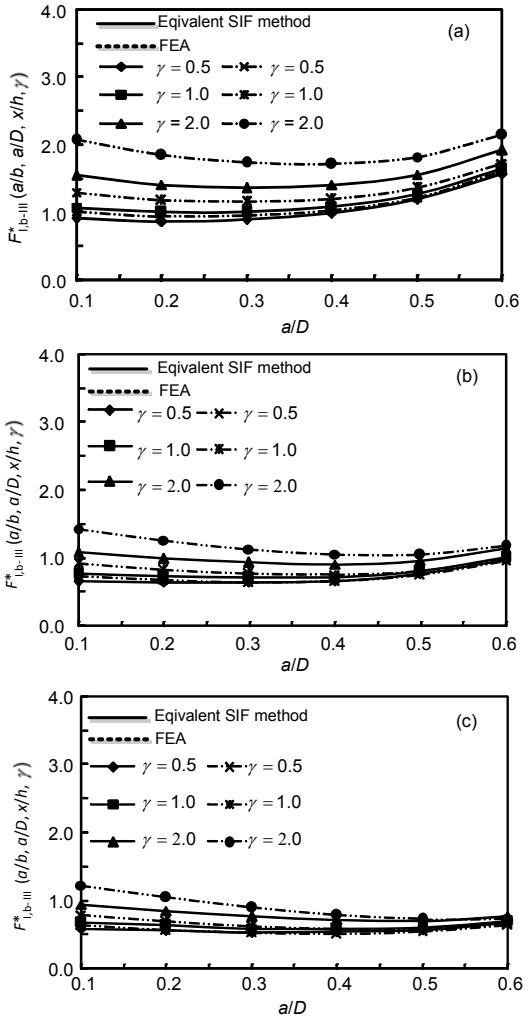

Fig. 12 Behavior of normalized stress intensity factors under combined loadings, $F^*_{\mathrm{I,b\text{-}III}}$ plotted against relative crack depths, a/D for three crack aspect ratios, (a) a/b=0.2, (b) a/b=0.6 and (c) a/b=1.0 at x/h=0.0 using different loading ratio, γ

$\gamma \geq 2.0$. When a/b increased, the discrepancies between the results were greatly reduced and all the $F^*_{\text{I,b-III}}$ values converged to the single value which occurred at a/D=0.6 (Figs. 12b and 12c). The discrepancies between combined SIFs obtained through different approaches are discussed below in relation to crack face interactions.

6 Crack deformation mechanisms

Figs. 13 to 15 show the stress distribution around the tip that is situated at the outer surface. Figs. 13 and 14 include the deformed meshes of the cracks subjected to pure torsion and bending moments, respectively. The SIFs from Figs. 13 and 14 are shown in Fig. 11, obtained at x/h=0.0. Clearly, the crack faces are completely closed when the cracks are subjected to torsion loading, whereas the crack faces subjected to bending moment are open (Fig. 14). The situation in Fig. 15 was then reproduced using the FEA subjected to a combined loading. Obviously, under combined loadings, the crack faces are open even in the presence of the torsion moment. The behavior of the crack face mechanism was responsible for producing the discrepancies between the results obtained using the two distinct methods.

In the FEA, the SIFs were calculated by referring to the relative distance between the two nodes situated on the crack faces. It is important to note that under the combined loadings, F^*_{FE} was found to be greater than F^*_{EQ} due to the fact that longer relative node distances were produced under combined loadings compared to the single loading. Therefore, ANSYS had calculated a greater F_{III} compared to the F_{III} obtained under complete closed crack faces subjected to pure torsion loading. By comparing the dimensionless SIFs obtained under a single loading as depicted in Figs. 7 and 9, $F_{\text{I,b}}$ was greater than F_{III}.

If γ=0.5 was used in the analysis, the torsion stress was half of the bending stress, producing larger crack face displacement or wider crack opening distances. This affected the value of F_{III} compared with the F_{III} obtained under pure torsion moments where the crack faces were found to be completely closed. Therefore, if F_{III} under pure torsion was used to combine with $F^*_{\text{I,b}}$ through Eq. (14), a lower combined SIF, $F^*_{\text{I,b-III,EQ}}$ was obviously produced compared with the combined SIF, $F^*_{\text{I,b-III,FE}}$ directly

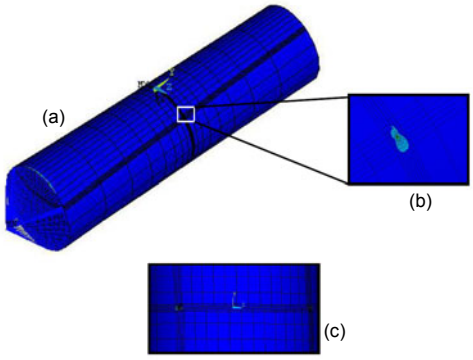

Fig. 13 Deformed meshes under torsion moment
(a) Whole model; (b) Crack tip; (c) Surface crack

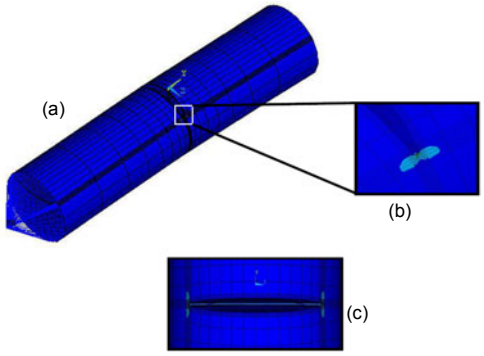

Fig. 14 Deformed meshes under bending moment
(a) Whole model; (b) Crack tip; (c) Surface crack

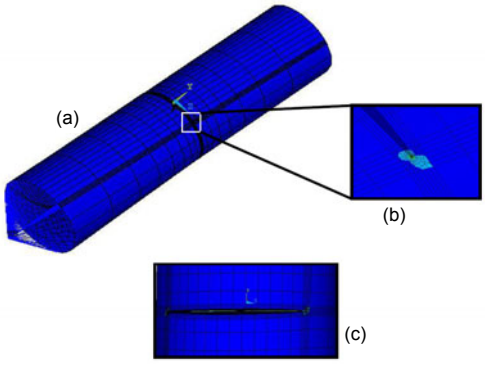

Fig. 15 Deformed meshes under combined loadings
(a) Whole model; (b) Crack tip; (c) Surface crack

obtained using FEA (Fig. 12a). If γ=2.0 was used, the shear stress was twice as great as the bending stress. This meant that less bending stress was allocated to open the crack faces. The stress condition in the bar was dominated by torsion moment, meaning that this condition was closely related to pure torsion moment. However, the SIF due to the bending moment was insignificantly affected by the combined SIF, $F^*_{\text{I,b-III}}$,

(Fig. 12c), where the combined SIFs, $F^*_{\text{I,b-III}}$, were almost in agreement with each other.

7 Conclusions

FEA were performed for semi-elliptical surface cracks in round bars under combined torsion and bending loadings. No published solutions were found to calculate the normalized SIFs, especially under the combined loadings. It had been assumed that the SIFs could be directly combined. Based on the findings of this study, the direct SIF combinations were rather questionable and inappropriate when different modes were involved, when compared with FEA results. The discrepancies in the results between the explicitly combined SIFs and the SIFs obtained using FEA were due to the different crack opening mechanisms shown by the deformed meshes, in which the crack faces were closed under pure torsion. The crack faces were opened under combined loadings even in the presence of torsion moments. The opening crack faces under the combined loadings increased the relative node distances. ANSYS then used these relative distances to calculate the SIFs. As a result, a higher F^*_{FE} was obtained, relative to the F^*_{EQ} due to the different mechanisms of crack deformation.

References

Agrawal, A., Karlsson, A.M., 2006. Obtaining mode mixity for a bimaterial interface crack using the virtual crack closure technique. *Journal of Fracture*, **141**:75-98. [doi:10.1007/s10704-006-0069-4]

Alshoaibi, A.M., Ariffin, A.K., 2006. Finite element simulation of stress intensity factors in elastic-plastic crack growth. *Journal Zhejiang University-SCIENCE A*, **7**(8):1336-1342. [doi:10.1631/jzus.2006.A1336]

Alshoaibi, A.M., Hadi, M.S.A., Ariffin, A.K., 2007. An adaptive finite element procedure for crack propagation analysis. *Journal of Zhejiang University-SCIENCE A*, **8**(2):228-236. [doi:10.1631/jzus.2007.A0228]

ANSYS, 2007. Release 11.0 Documentation. ANSYS Inc.

Aslantas, K., 2003. A different approach for calculation of stress intensity factors in continuous fiber reinforced metal matrix composites. *Journal of Solids and Structures*, **40**:7475-7481. [doi:10.1016/j.ijsolstr.2003.09.002]

Aslantas, K., Ergun, E., Tasgetiren, S., 2006. A numerical model for calculation of stress intensity factors in particle-reinforced metal-matrix composites. *Journal of Mechanical and Materials Design*, **3**:201-208. [doi:10.1007/s10999-007-9023-5]

Carpinteri, A., 1992. Elliptical-arc surface cracks in round bars. *Fatigue and Fracture of Engineering Materials and Structures*, **15**:1141-1153. [doi:10.1111/j.1460-2695.1992.tb00039.x]

Carpinteri, A., 1993. Shape change of surface cracks in round bars under cyclic axial loading. *Journal of Fatigue*, **15**:21-26. [doi:10.1016/0142-1123(93)90072-X]

Carpinteri, A., Vantadori, S., 2009. Sickle-shaped cracks in metallic round bars under cyclic eccentric axial loading. *Journal of Fatigue*, **1531**:759-765. [doi:10.1016/j.ijfatigue.2008.03.006]

Carpinteri, A., Brighenti, R., Vantadori, S., 2006. Surface crack in notched round bars under cyclic tension and bending. *Journal of Fatigue*, **1528**:251-260. [doi:10.1016/j.ijfatigue.2005.05.006]

Fonte, M.D., Freitas, M.D., 1999. Stress intensity factor for semi-elliptical surface cracks in round bars under bending and torsion. *Journal of Fatigue*, **1521**:457-463. [doi:10.1016/S0142-1123(98)00090-5]

Gray, G.T., Thompson, A.W., William, J.C., 1985. Influence of microstructure on fatigue crack initiation in fully pearlitic steels. *Metallurgical Transaction A*, **16**:753-760. [doi:10.1007/BF02814826]

Ismail, A.E., Ariffin, A.K., Abdullah, S., Ghazali, M.J., 2011. Off-set crack propagation analysis under mixed-mode loadings. *Journal of Automotive Technology*, **12**(2):225-232. [doi:10.1007/s12239-011-0027-7]

Lei, Y., 2004. *J*-integral and limit load analysis of semi-elliptical surface cracks in plates under combined tension and bending. *Journal of Pressure Vessels and Piping*, **81**(1):31-41. [doi:10.1016/j.ijpvp.2003.12.003]

Lin, X.B., Smith, R.A., 1997. Shape growth simulation of surface cracks in tension fatigue round bars. *Journal of Fatigue*, **19**:461-469. [doi:10.1016/S0142-1123(99)00075-4]

Mahmoud, K.M., 2007. Fracture strength for a high strength steel bridge cable wire with a surface crack. *Theoretical Applied Fracture Mechanics*, **48**:152-160. [doi:10.1016/j.tafmec.2007.05.006]

Qian, J., Fatemi, A., 1996. Mixed mode fatigue crack growth: A literature survey. *Engineering Fracture Mechanics*, **55**:969-990. [doi:10.1016/S0013-7944(96)00071-9]

Raju, I.S., Newman, J.C., 1986. Stress Intensity Factors for Circumferential Surface Cracks in Pipes and Rods under Tension and Bending Loads. Elsevier Science Publisher, North Holland, p.789-805.

Shahani, A.R., Habibi, S.E., 2007. Stress intensity factors in a hollow cylinder containing a circumferential semi-elliptical crack subjected to combined loading. *Journal of Fatigue*, **1529**:128-140. [doi:10.1016/j.ijfatigue.2006.01.017]

Shin, C.S., Cai, C.Q., 2004. Experimental and finite element analyses on stress intensity factors of an elliptical surface crack in a circular shaft under tension and bending. *International Journal of Fracture*, **129**:239-264. [doi:10.1023/b:frac0000047784.23236.7d]

Toribio, J., Matos, J.C., Gonzalez, B., Escuadra, J., 2008. Numerical modeling of crack shape evolution for surface flaws in round bars under tensile loading. *Engineering Failure Analysis*, **16**:618-630. [doi:10.1016/j.engfailanal.2008.02.014]